Comparison of kink-band structures and specificities of cell wall polysaccharides in modern and ancient flax fibres

Camille Goudenhooft, Alessia Melelli, Sylvie Durand, Xavier Falourd, Lucie Le-Bot, Loren Morgillo, Sanaa Gaballah, Roberta Cortopassi, Anita Quiles, Darshil U Shah, et al.

Carbohydrate Polymers 344 (2024) 122526

Contents lists available at ScienceDirect

Carbohydrate Polymers

journal homepage: www.elsevier.com/locate/carbpol

Comparison of kink-band structures and specificities of cell wall polysaccharides in modern and ancient flax fibres

Camille Goudenhooft [a,*], Alessia Melelli [b], Sylvie Durand [c], Xavier Falourd [c,d], Lucie Le-Bot [c], Loren Morgillo [a], Sanaa Gaballah [e], Roberta Cortopassi [f], Anita Quiles [e], Darshil U. Shah [g], Frédéric Jamme [b], Johnny Beaugrand [c], Alain Bourmaud [a]

[a] Univ. Bretagne Sud, UMR CNRS 6027, IRDL, Lorient, France
[b] Synchrotron SOLEIL, DISCO beamline, Gif-sur-Yvette, France
[c] INRAE, UR1268 BIA Biopolymères Interactions Assemblages, 44316 Nantes, France
[d] INRAE, BIBS facility, PROBE infrastructure, 44316 Nantes, France
[e] Institut Français d'Archéologie Orientale du Caire, Le Caire, Egypt
[f] Musée du Louvre, Département des Antiquités Egyptiennes, 75058 Paris, cedex 1, France
[g] Centre for Natural Material Innovation, Department of Architecture, University of Cambridge, Cambridge CB2 1PX, United Kingdom

ARTICLE INFO

Keywords:
Archaeological textiles
AFM
NMR
Biochemical composition
Deep-UV fluorescence
Mechanical properties

ABSTRACT

Flax (*Linum usitatissimum* L.) is a plant of industrial importance, its fibres being presently used for high-value textile applications, composite reinforcements as well as natural actuators. Human interest in this fibre-rich plant dates back several millennia, including to Ancient Egypt where flax was used extensively in various quotidian items. While the recent technical developments of flax fibres continue to diversify through scientific research, the historical use of flax also has rich lessons for today. Through careful examination of ancient Egyptian and modern flax fibres, this study aims to conduct a multi-scale characterization from the yarn to the fibre cell wall scale, linking differences in structure and polysaccharide content to the mechanical performance and durability of flax. Here, a multi-scale biochemical study is enriched by scanning electron microscopy and nanomechanical investigations. A key finding is the similarity of cellulose features, crystallinity index and local mechanical performances between ancient and modern fibres. Biochemically speaking, monosaccharides analysis, deep-UV and NMR investigations demonstrate that ancient fibres exhibit less pectins but a similar hemicellulosic content, especially through uronic acids and galactose, suggesting the sensitivity of these non-crystalline components.

1. Introduction

Flax (*Linum usitatissimum* L.) is a plant of industrial importance, its fibres being presently used for high-value textile applications, composite reinforcements and as natural actuators (Le Duigou & Castro, 2016), and the technical developments of flax fibres continue to diversify propelled by scientific research. While the use of flax fibres goes back well before the plant's domestication around 8.000 BCE (van Zeist & Bakker-Heeres, 1975), the flax fibre crop was cultivated for its fibres during the times of Ancient Egypt in the Nile valley (Heer, 1873). In ancient Egypt, flax was used for clothing, fishing nets, mortuary linen and also mummy stripes (Melelli, Shah, et al., 2021; Vogelsang-Eastwood, 2000). Flax has thus weaved its way through history, making it a material rich in lessons for today's progresses; indeed, some pieces of these precious textiles have been preserved through the ages, making it possible to study them using contemporary tools and to draw parallels with the modern fibres.

In plant stems, single flax fibres are aggregated in bundles of several tens of fibres located at the periphery (phloem) of the stems, glued together by the pectic middle lamellae (Melelli, Arnould, et al., 2020). After textile processing steps, including plant retting, fibre extraction, spinning and weaving, fibres are generally clean and without any cortical or middle lamellae residue. It is especially the case for ancient flax fibres, where the sensitive middle lamellae degrade further due to long-term ageing, following initial efficient but uncomplete removal by water retting commonly used in Ancient Egypt (André, 1964). These insights were clearly demonstrated in a previous paper through a deep

* Corresponding author.
E-mail address: camille.goudenhooft@univ-ubs.fr (C. Goudenhooft).

https://doi.org/10.1016/j.carbpol.2024.122526
Received 27 February 2024; Received in revised form 18 July 2024; Accepted 19 July 2024
Available online 20 July 2024

investigation of the yarn structure on a sample from a mortuary linen (Melelli, Shah, et al., 2021). Regarding the ultrastructure and properties of cell walls, a good preservation of mechanical performances was demonstrated after 4000 years of ageing but evolution in cell wall biochemical properties was not addressed in the study.

Flax fibres have a hierarchical and specific architecture: they are long fibres (20–40 mm)(Baley et al., 2018) with multi-layer organization (Primary cell wall, S1, S2 (also called G) and eventually S3 (also called Gn)), the main layer being S2 (or G) layer characterized by a high content in crystalline cellulose embedded in a matrix of non-cellulosic polymers (NCP) including structural hemicelluloses and pectic matrix (Goudenhooft et al., 2019; Rihouey et al., 2017). This specific layer confers to the fibre performing mechanical properties thanks to a very low microfibrillar angle (close to 5°) and high cellulose content (Melelli, Jamme, et al., 2020). Their low lignin content (between 1 and 2 %) and significant content in NCP make the flax fibres sensitive to ageing and especially to humidity and temperature, inducing swelling (Garat et al., 2020), structural changes (Gassan & Bledzki, 2001) and impact on mechanical performances (Siniscalco et al., 2018). In addition, presence of humidity may induce development of bacteria and fungi increasing the structural degradation (Caneva et al., 2005); the role of the lumen in biological degradation of the fibre was demonstrated by both Basu and Ghose (Basu & Ghose, 1962) and Melelli et al. (Melelli, Pantaloni, et al., 2021), with the lumen acting as a tunnel, facilitating the dissemination of water, fungi and bacteria.

Ageing of plant fibres can be examined through changes in ultrastructure, biochemical composition and mechanical performance. Quantification of sugars is an informative technique to compare changes in plant fibre composition at the micro-scale. In recent years, biochemical composition analysis has been extensively used to compare plant fibres of different species, and even investigate the consequences of drought (Melelli et al., 2022), physical treatments (Gautreau et al., 2021) or verticilliose disease (Nuez et al., 2022). To finely explore changes in cellulose ultrastructure, solid-state NMR (Nuclear Magnetic Resonance) is a technique that enables the investigation of the supramolecular organization of polysaccharide assemblies without prior modifications, thereby allowing the comparison of samples of different natures and monitoring process effects. Its utility has been demonstrated in tracking changes in cellulose structure and organization induced by flax retting processes (Bourmaud, Siniscalco, et al., 2019) and, moreover, the impact of water stress (Melelli et al., 2022) on the organization of cellulose and hemicellulose. Solid-state NMR and sugar composition analysis can also be supplemented by microscopy or other spectroscopy methods to provide local information or mapping of properties. Synchrotron beamlines provide original and powerful tools such as deep-UV fluorescence micro-spectroscopy. Indeed, the autofluorescence of plant cell wall components such as protein, lignin or phenolic compounds can provide rich information about local composition; it demonstrated its potential on flax cell walls (Beaugrand et al., 2022) but also on historical artefacts such as ancient lutes from wood (Echard et al., 2015).

Local mechanical properties can also be a good indicator of cell wall ageing. Nanoindentation and AFM (Atomic Force Microscopy) are powerful techniques for characterizing fibre mechanical performances at the cell wall level. Indeed, AFM can be used in peak-force quantitative nano-mechanical property mapping (PF-QNM) mode to determine the indentation modulus of different types of materials, including plant fibres (Bourmaud, Mérotte, et al., 2019). In the case of flax, AFM has been used to illustrate gradients in mechanical properties according to the fibre maturity (Goudenhooft et al., 2018), the retting degree (Bourmaud, Siniscalco, et al., 2019), the effects of ageing of paintings on canvas (Melelli, Roselli, et al., 2021) as well as to measure changes in fibre properties during degradation by composting (Melelli, Pantaloni, et al., 2021). Nanoindentation is also sometimes used in the cultural heritage field to address changes in mechanical behaviour, for example, Salvant et al. investigated ageing of paint oils through nanoindentation tests (Salvant et al., 2011) and Tiennot et al. used the technique to evidence heterogeneities in paint layers of a 17*th*-century Dutch painting (Tiennot et al., 2020).

In the present study, the state of preservation of an ancient flax textile of interest is investigated and compared with a modern reference sample. Here, we examine the composition, ultrastructure and mechanical characteristics of flax fibres from a 4000-year-old ancient Egyptian mortuary fabric, from the yarn scale to the fibre cell walls. First, a morphological study of flax fibres through SEM analysis is addressed and the biochemical properties are investigated through three different approaches. At fibre scale, sugar analysis explores the monosaccharide contents after long-term ageing. NMR and Deep UV investigations give precise information on cellulose structure and components mapping at cell wall scale, respectively. The last section of the paper is dedicated to a comparison of local mechanical performances estimated by AFM and discussed in relation to the biochemical results.

2. Material and methods

2.1. Flax samples

An ancient Egyptian textile and a contemporary flax yarn, referred to as ancient and modern flax respectively, were studied. The ancient sample derives from a large flax fabric bordered with a fringe (inv. E 13595) archived at Le Louvre Museum (France). Information about the provenance of the Egyptian textile and morphological characteristics are mentioned in the work of Melleli et al. (Melelli, Shah, et al., 2021). This ancient flax fabric was radiocarbon dated (Laboratoire de Mesure du Carbone 14, SacA70167, CEA-Saclay, Gif-sur-Yvette, France) between 4324 and 4053 cal. BCE with 95.4 % probability, indicating that flax plants were harvested and fibres extracted from a period known as the First Intermediate Period and the beginning of the Middle Kingdom. For comparison, a contemporary yarn was analysed. This later was obtained from plants of several varieties cultivated in Normandy (France) by Teillage Saint-Martin company and dew-retted, in 2018. The company also performed scutching, hackling and stretching prior to spinning by Safilin Pionki. Additional information about morphological characteristics is mentioned in the previous work of Melelli et al. (Melelli, Shah, et al., 2021).

2.2. SEM observations

A few millimetres of yarn per sample was used and glued on a conductive adhesive. Prior to observation, a thin layer of gold was deposited on the sample using an Edwards Scancoat Six metallization device for 180 s. Then, a Jeol JSM 6460LV scanning electron microscope was used to analyse the flax samples, based on secondary emission electrons and an accelerating voltage of 3.0 kV.

2.3. Deep UV (DUV) fluorescence – DISCO beamline

A few millimetres of each yarn were cut and dehydrated with ethanol cycles before being embedded in paraffin, then cut to obtain cross-sections of 10 μm thick as described in a previous work (Melelli et al., 2022). The cross-sections were placed in fused quartz glasses and stored until the analysis session.

At Synchrotron SOLEIL DISCO beamline, two microscopes were used to perform DUV analyses: a wide field microscope for multi-spectral imaging (TELEMOS) and a point scanning microscope coupled with a spectrometer for mapping (POLYPHEME). To calibrate both microscopes, a small window of luminescent reference compound (Nd-YAG crystal) was used to obtain the maximum counts and adjust the focus. Samples were exposed to DUV radiation in the low microwatt range, which limits photodegradation.

2.3.1. Widefield multi-spectral microscope (TELEMOS)

The UV light was extracted from the white beam and

monochromatized thanks to a Czerny-Turner monochromator (iHR320, Jobin-Yvon, France) before reaching the end-station (Jamme et al., 2010). The widefield microscope used is a full field Axio Observer Z1 inverted microscope (Carl Zeiss GmbH, Germany) modified with quartz optics and coupled with a back-illuminated CCD 16-bit camera (Andor iKon-M camera) and a motorised sample plate (MS-2000 XY, Applied Scientific Instrument, USA). An Ultrafluar 40× (N.A.0.6) Glyc (Zeiss) objective with chromatic correction was used to investigate the samples, reaching a projected pixel size of 250 nm. A Semrock FF310-Di01 dichroic mirror was used to select the spectral range from approximately 300 nm (40%T) to 600 nm (%$T > 90$). In this paper, we focus our attention on three mains bandpass Semrock BrightLine® fluorescence filters that specifically select the range of tryptophan and tyrosine emissions (329–351 nm), ferulic acid (380–420 nm) and the range with a combination of the emission of caffeic acid and lignin (420–480 nm) (Jamme et al., 2013; Vidot et al., 2019). The excitation wavelength was set at 275 nm and the exposure time was set at 30s, 10s and 10s respectively to obtain the best signal-to-noise ratio while avoiding signal saturation or bleaching.

The images were successively pre-processed as illustrated in Beaugrand et al., 2022 (Beaugrand et al., 2022) and Melelli et al., 2022 (Melelli et al., 2022) by ImageJ. Two different areas of two cross sections (a cross-section of the ancient flax yarn and a cross-section of the modern yarn) were investigated. For each area of the samples analysed, at least three ROIs including one or more fibres were manually created with ImageJ selection tools to extract the fluorescence intensity emitted in each range selected through the three emission filters.

2.3.2. Fluorescence microspectroscopy with the hyperspectral microscope (POLYPHEME)

The microscope is an Olympus IX71 inverted micro-spectrofluorimeter modified with quartz optics to perform deep-UV analyses. The spectrometer has a 0.5 nm spectral resolution and a triple monochromator (T64000, Jobin-Yvon) in subtractive mode is used to suppress Rayleigh scattering. The fluorescence emission is collected by an iDus CCD detector (Andor) of 1024 × 256 pixels with a 26 × 26 μm pixel size. The objective chosen was an Ultrafluar 40× (N.A.0.6) glycerol immersion objective (Zeiss) and the beam spot diameter obtained was approximately 4 μm. An excitation wavelength of 275 nm was selected, and the centre of the spectrum window was set at 420 nm to acquire a range of spectral emission between 290 and 545 nm. The acquisition time was set at 10 s, and the accumulation was set at 1. Spectral maps were acquired every 2 μm step size. After the data acquisition, the spectra were preprocessed through MATLAB homemade scripts to correct spikes and dead pixels (Poulon et al., 2017) and all the spectra were extracted from 302 nm to 520 nm to avoid signals due to the beam reflection and the second harmonic at 550 nm. Quasar open access software (Toplak et al., 2017, 2021) was used to normalize the spectra with the area normalization method closest value selected between 370 and 380 nm and to exclude outliers. This normalization method was chosen among others because it keeps the ratios of the peaks of a spectrum almost unchanged. Past3 (Hammer et al., 2001) open software was used to build the principal component analysis (PCA) model considering all the corrected spectra of three fluorescence maps, two maps taken from the modern flax in different areas and one map taken from the ancient flax yarn.

2.4. Biochemical composition

The samples were analysed following the procedure described in Melelli et al. (Melelli et al., 2022). Briefly, first, the samples are cryo-ground in nitrogen liquid (SPEX 6770Freezer Mill) for homogenisation purpose. Then, wet chemistry (monosaccharide, lignin, protein content analysis) was conducted on the homogenised powder.

2.4.1. Monosaccharides

Neutral monosaccharides were analysed as their alditol acetate derivatives (Blakeney et al., 1983) by gas chromatography-flame ionization detection (GC-FID) (Perkin Elmer, Clarus 580, Shelton, CT, USA). Acidic monosaccharides also called uronic acids were analysed following the protocol described in (Guillou et al., 2023) using the Blumenkrantz & Asboe-Hansen method (Blumenkrantz & Asboe-Hansen, 1973). Hot sulfuric acid hydrolysis transforms the polysaccharides into furfural derivatives. Reaction with Orcinol (3,5-dihydroxytoluol) and MHDP (meta-hydroxydiphenyl) forms complex components measured by absorbance at 420 and 530 nm respectively using calibrations curves. Analyses were performed in three independent assays. The total monosaccharide content is the sum of each neutral and acidic monosaccharide amount.

2.4.2. Lignin

Lignin was assessed by spectrophotometry following the acetyl bromide method (Hatfield & Fukushima, 2005). The acetylation of lignin results in its solubilisation in acidic conditions. Next to amination reaction, lignin content is estimated by absorbance measurement at 280 nm using the extinction coefficient of 20 $L.g^{-1}.cm^{-1}$ mean value for herbaceous AcBr treated lignin (Fukushima & Hatfield, 2001; Iiyama & Wallis, 1990). Approximately 20 mg was weighted per assay. The analyses were performed in triplicate.

2.4.3. Proteins

Regarding the protein contents, the total N content was quantified based on approximately 3 mg of samples using an elemental analyser (VarioMicro, Elementar). Then, protein contents were calculated from the N content multiplied by a 5.7 coefficient, a number well known for non-reserve proteins. Experiments were run in triplicate with a calculated experimental error.

2.5. NMR analysis

Approximately 80 mg of each sample were rehydrated to 38 +/− 2 % (*w*/w) with ultra-pure water. The solid-state NMR spectra were carried out on a Bruker Avance III 400 MHz spectrometer operating at a carbon frequency of 100.62 MHz. A double resonance $^{1}H/X$ CP/MAS 4 mm probe coupled with a high-power level amplifier was used for ^{13}C CP/MAS experiment. The magic angle spinning (MAS) rate was set at 12 kHz and each acquisition was acquired at ambient temperature (298 K). The experiment was conducted under a 90° proton pulse of 3.3 +/− 0.1 μs, a contact time of 1.5 ms and a 10 s recycling time. Each spectrum was the result of the accumulation of 2048 scans. Chemical shifts were calibrated using glycine as external reference, assigning the carbonyl at 176.03 ppm. We employed the advanced approach developed by Larsson et al., (Larsson et al., 1997) which has been utilized multiple times (Bourmaud, Siniscalco, et al., 2019; Newman et al., 2012; Zuckerstätter et al., 2009) to determine the crystallinity and overall morphology of the samples. This method, based on C_4 signal processing used four lines for the crystalline part and three lines for the amorphous part. In the crystalline part, three Lorentzian lines correspond to cellulose Cr (Iα) (88.7–88.8 ppm), cellulose Cr (Iα + β) (88.2 ppm) and cellulose Cr (Iβ) (87.5–87.6 ppm). Additionally, a Gaussian line was assigned to represent the paracrystalline (PCr) contribution (87.9 ppm). In the amorphous part, two Gaussian lines correspond to accessible surface (AS; 82.6 and 83.6 ppm) while one represented the inaccessible surface (IAS; 82.9–83.1 ppm).

The chemical shifts, half width and area of peak of samples were determined using a least-squares fitting method with the Peakfit® software (Systat software Inc., USA). The cellulose crystallinity was assessed by calculating the peak area ratio of four lines representing the crystalline portion to seven lines for the cellulose C_4 region. Utilizing NMR signal areas from the amorphous cellulose compared to the total cellulose surfaces, along with a microfibril model comprising cellulose

chains with a width of 0.57 nm (Newman, 1999), the lateral fibril dimensions (LFD) and the lateral fibril aggregate dimension (LFAD) can be determined. This assessment considers a square cross-sectional cellulose microfibril model for NMR analysis.

The relative proportion of hemicelluloses (HC) was estimated from the cluster associated with the C_1 of polysaccharides. The area of the peak associated with hemicelluloses (100.9 ppm) was divided by the total area of the C_1 cluster to assess the proportion of HC in the samples.

The molecular dynamic of samples was further characterized by varying contact time (τ) from 10 μs to 9000 μs. Twenty CP/MAS spectra were recorded with an accumulation of 512 scans per contact time. The evolution of carbon peak area (C_4 of crystalline cellulose and C_4 of amorphous cellulose) in function of contact time was fitted with eq. (1) as previously (Lahaye et al., 2023):

$$I(\tau) = I_0 e^{-\tau} \Big/ T_{1\rho}^{H} \left(1 - \lambda e^{-\tau} \Big/ T_{HH} - (1-\lambda) e^{-3\tau} \Big/ 2T_{HH} \times e^{-\tau^2} \Big/ 2T_{CH}^2\right)$$

where, I(τ) is the intensity of the carbon peaks as a function of contact time, I_0 the theoretical maximum intensity in the absence of relaxation, τ the contact time, T_{HH} is the spin diffusion time, λ relates to the number of ^1H bound to ^{13}C. $T_{1\rho}^{H}$ is the spin lattice relaxation time in the rotating frame.

Another approach based on Bardet et al. works (Bardet et al., 2012) was applied based on eq. (2):

$$I(\tau) = I_{0a}(1 - e^{-\tau}/T_{CHa})\left(e^{-\tau}/T_{1\rho a}^{H}\right) + 1_{0b}(1 - e^{-\tau}/T_{CHb})\left(e^{-\tau}/T_{1\rho b}^{H}\right)$$

This leads to two values for T_{CH} and $T_{1\rho}^{H}$, weighted by their respective proportions and leading to the following interpretations: when $T_{1\rho}^{H}$ values are similar, this reflects a single proton pool and a homogeneous sample at the nanoscale. If the $T_{1\rho}^{H}$ values differ, the structure is not homogeneous at the nanoscale and at least two spatial domains can be distinguished.

2.6. Nano-mechanical investigations

2.6.1. Preparation of samples

A subsample of <5 mm was cut for each sample. These subsamples were embedded in Agar resin (epoxy resin Agar Low Viscosity Resin (LV) - Agar scientific UK) and put in an oven at 60 °C overnight for the resin polymerization. Resulting blocks were then machined to reduce their cross-section and glued on an AFM stainless steel mounting disk. Then, the sample surface was trimmed with an ultramicrotome (Ultracut S, Leica Microsystems SAS, France) equipped with diamond knives (Trim and Ultra AFM, Diatome, Switzerland) to remove thin sections (60 nm thick for the final step) at reduced cutting speed (~1 mm/s).

2.6.2. Nanoindentation

Nanoindentation measurements were performed at room temperature on both samples with a Nanoindenteur XP (MTS Nano Instruments, Oak Bridge, Tennessee, USA) equipped with a three-side pyramid indenter (Berkovich Berko XPT-12761-0). Once the indenter touched the surface, the strain rate was set at 0.05 s^{-1} (i.e., 1 μN/s) during loading up to a depth limit of 120 nm. Then, the load was held for 60s at the maximum value and finally the withdraw was done with the same loading rate up to 10 % of the maximum load. Both indentation modulus and hardness were calculated through contact theory and equations developed by Oliver and Pharr (Oliver & Pharr, 1992).

2.6.3. AFM PF-QNM investigations

A Multimode 8 Atomic Force Microscope (Bruker, Billerica, Massachusetts, USA) was equipped with a RTESPA-525 probe (Bruker probes, Billerica, Massachusetts USA) with a resonance frequency of 525 kHz and a nominal spring constant of 200 N/m. The actual spring constant was calculated with the Sader Method (https://sadermethod.org/). The AFM set-up was calibrated with the relative method using sapphire as hard standard material to calculate the deflection sensitivity and the PF-QNM synchronization distance. A sample of aramid fibres K305 Kevlar Taffetas 305 g/m^2 (Sicomin epoxy systems, France) prepared with the same protocol as the flax samples and previously tested by nano-indentation, was used to calibrate the tip radius. The stiffness of the cantilever used was between 158 N/m and the tip radius between 50 and 60 nm over the measurements.

The fast scan axis angle was at 90°, the maximum of the peak force setpoint used was 200 nN and the oscillation frequency selected at 2 kHz. The Poisson's ratio used was set to 0 to obtain the raw indentation modulus and not the Young's modulus, obtained through the AFM software and not pertinent here due to the high anisotropy of flax fibres (Delafargue & Ulm, 2004; Jäger et al., 2011). The maximum fast scan velocity was selected at 4 μm/s for the fibres and 0,445 μm/s for the focus in the cell walls, and the image resolution set to 256 × 256 pixels. To obtain the indentation modulus values of flax fibres, the surface of the cell wall of each fibre was selected from the images and indentation moduli were obtained for each selected point using Gwyddion free software (http://gwyddion.net/).

3. Results and discussion

3.1. From the yarn macro to the fibre microscale

3.1.1. Investigation of the fibre specificities through SEM analysis

At the yarn macroscale, Melelli et al. showed a high degree of fibre individualization in the ancient yarn, mainly composed of elementary fibres with very few cortical residues or bundles with middle lamellae, whereas the modern flax yarn exhibited numerous residues including middle lamellae and cortical parenchyma (Melelli, Shah, et al., 2021). As a complement, the SEM micrographs in Fig. 1. M1 and A1 show the overall aspects of modern and ancient fibres, respectively, within the yarns. At this scale, the surface of modern fibres seems quite smooth and homogeneous, and only a small number of defects – also called "kink-bands" – is visible (M1). For ancient fibres, many defects and heterogeneous areas can be observed (A1); at low magnification, ancient fibres exhibit a brittle behaviour with drastic changes of direction in kink-bands regions (A1), compared to modern ones which appear to have a higher flexibility (Melelli, Shah, et al., 2021). In addition, ancient fibres are observed to have lower diameters, already underlined in our previous work, probably due to the combined effects of water retting and associated disappearance in residual surface components, and varietal differences.

At the scale of one or a few fibres, it is possible to identify the well-known band-like shape of kink-bands in the modern fibres (M2-M3). Whereas for ancient fibres, a range of defect shapes are observed (A2-A5). While some characteristic band-like kink-bands are also visible in ancient fibres, the outer shell of the fibres looks degraded in these areas (A2); uncommon shapes of kink-bands can be observed too (A3), more "spread out" along the fibre and as if detached from the fibre at certain edges.

Cracks and wrinkle-like bulges (A4-A5) appeared on ancient fibres, i.e., defects that have not been observed on modern fibres in the present study and to our knowledge. At a higher magnification, the surface of modern fibres seems rather smooth and homogeneous despite the presence of the kick-band (M4). On the other hand, in the case of ancient fibres (A6-A7), the surface seems degraded and what the authors assume to be cellulose macrofibrils appear to be visible with an orientation close to the fibre axis, suggesting a possible alteration in primary cell wall (PCW) and S1 layer after long-term ageing.

3.1.2. Deep-UV fluorescence analysis

At the yarn macroscale, Deep-UV fluorescence analyses highlighted a significant difference in fluorescence emission between modern and ancient flax fibres. Fig. 2 presents two images in two different areas of modern (M1 and M2) and ancient (A1 and A2) flax yarns. Several

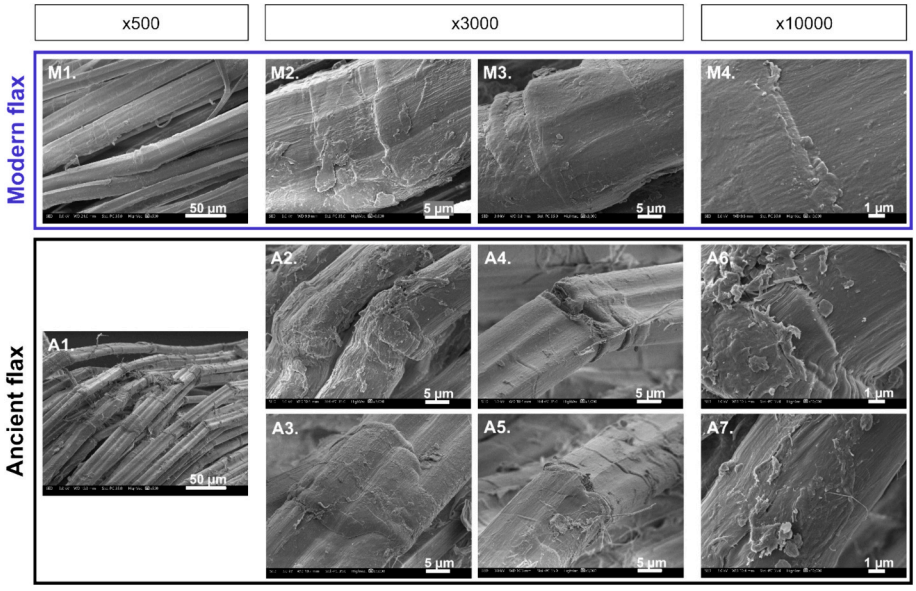

Fig. 1. SEM images of modern (in blue) and ancient (in black) flax yarns. Overview of fibres within the yarns (M1. and A1.); focus on different areas of heterogeneities or kink-bands (M2-M3 and A2-A5); higher magnification of some of the areas of heterogeneities (M4 and A6-A7).

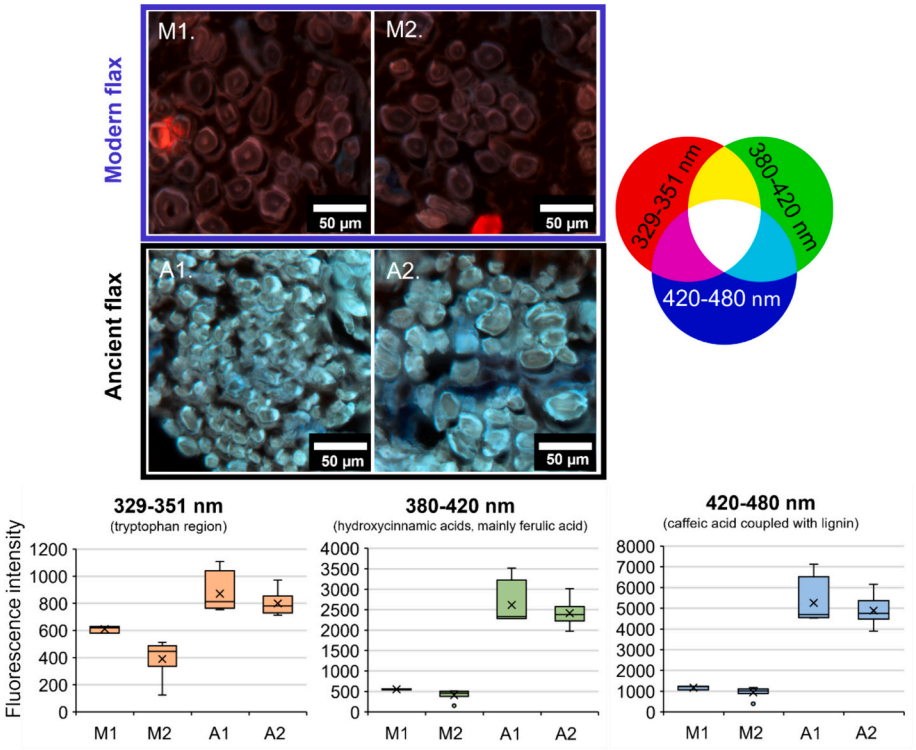

Fig. 2. Multi-spectral composite images in false colour obtained by merging three images collected with the three different bandpass filters (R:329–351 nm, G:380–420 nm, B:420–480 nm). Two different areas of a same cross-section were selected: M1-M2 for the modern yarn and A1-A2 for the ancient Egyptian yarn. At least 3 ROIs of each area investigated were selected to extract quantitative values of the fluorescence emission also illustrated in the three box plots representing the three bandpass filters separated. The ancient Egyptian yarn showed a higher fluorescent emission in all the ranges, but fluorescence of hydroxycinnamic acids and lignin resulted predominant in the ancient flax respect to modern flax, which gives a cyan colour. Display range values set for the images: R 0–2000, G 0–4000, B 0–8000.

regions of interests (ROIs) were selected from each image and the fluorescence intensities were extracted and quantified after an image pre-processing (Beaugrand et al., 2022; Melelli, Shah, et al., 2021).

Each of the four composite images were obtained by merging the three separate images collected with the three bandpass filters attributed to the tryptophan and tyrosine region (329–351 nm, red), the hydroxycinnamic acids mainly represented by ferulic acid (380–420 nm, green), and the caffeic acid coupled with lignin (420–480 nm, blue). The fluorescence intensity in the range assigned to tryptophan and tyrosine was expected to be lower in the ancient sample due to protein degradation over time. However, the intensity of the fluorescence emitted was significantly higher for the ancient Egyptian yarn across all three

bandpass filters. The composite image of the ancient Egyptian in Fig. 2 shows the cyan colour because of the predominance of fluorescence intensity due to the hydroxycinnamic acids and lignin, which hide the protein signal represented by the red channel. The Egyptian textile was found in a tomb and in a good state of preservation; the textile was probably a shroud or part of funerary object, and some contamination of exogenous origin, possibly by proteins, cannot be excluded. On the other hand, the optimal environmental conditions with constant humidity and temperature as well as the absence of light may have favourited the natural ageing without the impact of other degrading factors such as biodegradation. Tryptophan is known to be sensitive to its environment, such as the pH or the presence of heavy atoms such as iodide, bromide and halogenated compounds (Garidel et al., 2008; Lakowicz, 2006). Consequently, correlating its emission with protein degradation is challenging. Nevertheless, the increased fluorescence observed in aged yarn may also serve as an indicator of the increased textile acidity, which is a very common phenomenon on ancient fabrics linked to hydrolysis process (Peacock, 1983). The quenching effect of hemicellulose on lignin has been reported in other studies (Donaldson, 2020; Hafrén, 2007), and the high fluorescence emission due to lignin in the ancient Egyptian yarn could be explained by the degradation of NCPs of the fibre matrix, which in modern fibres quench the lignin signal but reveal the true fluorescence emission of lignin once they are degraded.

The higher fluorescence intensity of ferulic acid in the ancient archaeological yarn seems to support the degradation of NCPs since ferulic acid is linked to hemicellulose through ester bonds and can be released by esterase enzymes due to the action of microorganisms (Bugg et al., 2011). In addition, the ratio between the fluorescence emission generated by tryptophan and that of lignin, or between tryptophan and ferulic acid, is observed to be greater in modern yarns compared to ancient ones. This difference is visible in both multi-spectral images, where fluorescence emissions were quantified from their ROIs (box plots in Fig. 2), and in the analysis presented in Fig. 3, which includes maps and the result of principal components analysis obtained with the hyperspectral microscope. Using the PCs (principal components) 1 and 2 built with maps collected from the modern yarn and one map of the ancient yarn, two well-distinguished clusters can be observed. PC1 highlights the ratio between the contribution of proteins (300–360 nm) and the rest of the spectrum, where signals of ferulic (415–420 nm) and lignin (480–520 nm) are mainly observed. In PC1 all the variables between 400 and 520 are more important for the Egyptian yarn by forming a cluster shifted to positive values; contrarily to modern fibres that form a cluster mainly shifted to negative values. However, one should note that we can observe high heterogeneity in the ancient flax fibres and approximately half of the pixels, which also include the background due to paraffin, are in common with the modern flax.

PC2 highlights mainly the ratio between the contribution of proteins (300–360 nm) plus a broad emission of caffeic acid (440 nm) and lignin (at 480 nm) for positive values and those of the p-coumaric acid (400 nm) and the broad emission of lignin (at 495–520 nm) for negative values, confirming the results found with the multi-spectral images. Lignin is a very complex biomolecule and Day et al. (Day et al., 2005) observed the presence of different epitopes of lignin (guaiacyl-condensed, guaiacyl/syrigyl condensed, guaiacyl/syrigyl non-condensed) in flax bast fibres. The two opposite lignin signals in PC2 could evidence the biochemical modifications of an epitope rather than another, but further analyses focused on pure lignin samples are required to confirm this hypothesis.

3.1.3. *Biochemical analysis*

A biochemical analysis of the two types of fibres was performed to evaluate their content in monosaccharides or polysaccharides, lignin and proteins. Based on Table 1, and analysing first the content of monosaccharides, modern flax fibres are richer in galactose and uronic acids whereas ancient flax is richer in glucose (in %wt of dry matter but also in wt% of total sugar content). Moreover, when looking at the total amount of the monosaccharides, the ancient sample shows a much higher content, with glucose being the main contributor. These results lead to the interconnected discussions hereafter. It is also important to keep in mind that flax variety and associated intrinsic characteristics may vary; these changes can drastically impact the specific contents in biochemical components, adding an uncertainty to the following conclusions and assessments.

First, the glucose content exhibits a relative increase in wt% of dry matter, other components such as galactose and uronic acids being degraded. This is quantified by the Glc/NCP ratio shown in Table 1.

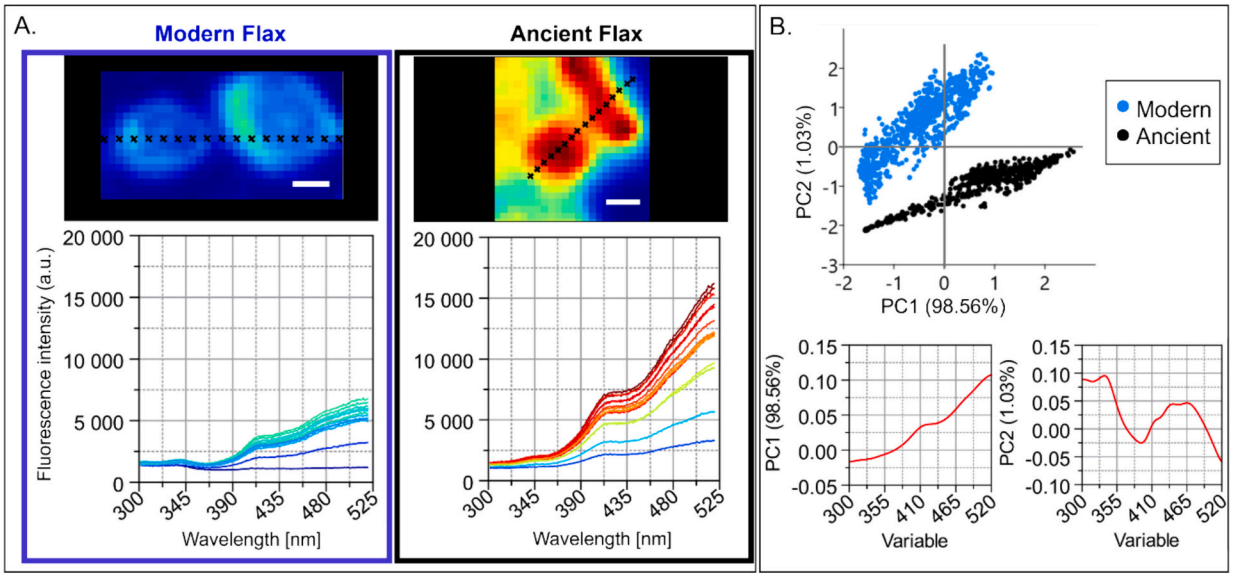

Fig. 3. A. Two spectral maps of modern and ancient flax yarns and the points illustrating the spectra extracted for the comparison in the graphics. Scale bar 10 μm. B. PCA model built considering all the spectra of three maps (two maps of modern flax and one map of ancient flax) with the relative loadings. The ancient Egyptian yarn has the highest fluorescence emission in the range of ferulic and lignin (PC1), while in modern yarn proteins are the most contributing variable. In PC2, the ratio between proteins (tyrosine and tryptophan) and lignin, with a small contribution of hydroxycinnamic acids, is even more crucial to distinguish the two clusters of samples with the ancient yarn having negative values.

Table 1
Monosaccharides, lignin and proteins contents (in wt% of dry matter, and in relative % for monosaccharides) for the modern and ancient samples. Ratios Glc/NCP and Gal/Rha are also reported. Ara: arabinose, Rha: rhamnose, Gal: galactose, Glc: glucose, Xyl: xylose, Man: mannose and NCP: non-cellulosic polysaccharides. NCP values are the sum of xylose, rhamnose, galactose, mannose and arabinose.

	wt% of dry matter				Relative % of monosaccharide expressed as % of total monosaccharide	
	Modern		**Ancient**		**Modern**	**Ancient**
	Mean	**SD**	**Mean**	**SD**		
Ara	1.12	0.11	0.98	0.04	1.3	1.0
Rha	0.26	0.03	0.72	0.15	0.3	0.7
Gal	3.82	0.19	0.58	0.02	4.5	0.6
Glc	69.57	1.95	90.90	0.31	82.7	91.6
Xyl	1.27	0.07	1.50	0.04	1.5	1.5
Man	4.28	0.09	4.97	0.23	5.1	4.3
Uronic acids (UA)	3.84	0.33	0.24	0.00	4.6	0.2
Total monosaccharides	84.16	1.88	99.19	0.00	100	100
Glc/NCP	6.48	0.25	11.3	0.48	N/A	N/A
Gal/Rha	14.66	1.83	0.82	0.14	N/A	N/A
UA/Rha	14.81	2.74	0.34	0.07	N/A	N/A
Lignin	2.6	0.2	3.4	0.1	N/A	N/A
Proteins	1.25	0.15	1.47	0.02	N/A	N/A

Moreover, monosaccharides related to hemicelluloses (Man, Xyl and Ara) shows a relative content rather comparable with modern flax.

In addition, galactose is known to be a major contributor to the holding of cellulose chains (Morvan et al., 2003) so their degradation could have an impact on the mechanical properties of the ancient yarn and also on the mechanical behaviour of the cell walls, decreasing the cellulose microfibril cohesion and inducing a brittle behaviour; this assessment is consistent with previous SEM analysis and especially the development of cracks (Fig. 1. A4-A5). Additionally, as explained in the study of Melelli et al. (Melelli et al., 2022), the ratio Gal/Rha is a good indicator of rhamnogalacturonan type-I RG-I and the average length of its side chains, with more RG-I long chain structuring pectins in modern flax (Gorshkova et al., 2010; Gorshkova & Morvan, 2006). Nevertheless, conclusions on possible differences in RG-I ramifications cannot be assessed here, because galactose is possibly linked to a large range of cell wall polymers such as RG-I, RG-II or arabinogalactans proteins, and the proportions of rhamnose substituted and unsubstituted by side chains cannot be determined through the monosaccharide composition without in depth polymer structural characterizations (Gautreau et al., 2022).

Uronic acids are known to be related to pectins and very sensitive to their environment (Lashermes et al., 2020); the lower uronic acid content in ancient fibres (16 times lower than in modern fibres) highlights the polygalacturonan polymers (PGA) degradation in the ancient yarn. In addition, one can notice the huge differences in UA/Rha ratio, which reaches the average of 0.34 and 14.81 for the ancient and modern flax, respectively. This underlines the strongly contrasted feature of pectic components in ancient flax with a more important ratio of short RG-I chains compared to long polygalacturonan polymers (PGA) being degraded in ancient flax.

In addition, the ancient sample is also richer in lignin, but this amount remains rather low (<3.5 % of the dry mass). When analysing the ratio Glc/lignin, 26.8 is obtained for the modern sample and 26.7 is calculated for the ancient yarn, showing that despite different absolute values, the ratio of glucose and lignin remains the same. Thus, the increase of lignin in wt% of dry matter in the ancient sample is also relative, the lignin being preserved whereas other more labile and sensitive components are degraded. As discussed in the previous 3.1.2 section, on modern flax, the fluorescence signal from lignin may be quenched by non-cellulosic polymers. Regarding proteins content, it is very similar between the two samples, hypothesizing, as previously suggested, a good preservation of proteins due to stable environment or possible exogenous contamination.

3.2. From the fibre microscale to the cell wall nanoscale

3.2.1. NMR investigations

To provide information at the nanoscale, the cell wall cellulose crystallinity of ancient and modern fibres was investigated by NMR. Fig. 4 shows the ^{13}C CP/MAS NMR spectra obtained for both samples.

The obtained ^{13}C CP-MAS spectra show a predominantly cellulosic material with a similar hemicellulosic content and less pectins (Newman & Redgwell, 2002), in agreement with the biochemical analysis previously mentioned. Indeed, considering the ratio of the area of the peak associated with hemicelluloses (~101 ppm) and the total area of the C_1 cluster, the same value of 8 % is obtained for both samples highlighting the similar hemicellulosic content. Additionally, the signal at ~32 ppm is clearly visible in the spectrum of the modern yarn, in contrast to the ancient yarn. This signal has previously been observed in flax samples (Bourmaud, Siniscalco, et al., 2019) and its concomitance with that of a peak at ~173 ppm (Fig. 4. B.) means that it can be attributed to a -COO$\underline{C}H_3$ of pectins. The much shorter peak at ~173 ppm for the ancient flax illustrates the lower content in pectins in the ancient sample. This is in agreement with FTIR results from the literature (Melelli, Shah, et al., 2021) as well as biochemical results from the present study previously mentioned in Table 1 and illustrated by the lower content of uronic acids but also lower ratio Gal/Rha in the ancient sample. Moreover, the difference for both signals related to pectins highlights a lower methyl esterification for the ancient sample compared to the modern one (Goldberg et al., 1996).

In addition, Table 2 gives information about the cellulose supramolecular organization, and provides structural information about degree of crystallinity and dimensions of lateral fibril (LFD) and associated aggregate (LFAD). As previously reported by (Melelli, Shah, et al., 2021), cellulose crystallinity is similar for both samples, with 58 % and 56 % respectively for modern and ancient yarns. Assuming that the crystallinity of the sample before ageing can be assimilated to that of the modern sample, the cellulose would demonstrate a good stability through ageing.

In addition, the two samples have similar lateral fibril dimensions (LFD) but different lateral aggregate dimensions (LFAD), with 30 nm and 20 nm respectively for the modern and ancient yarns. As a result, the average number of fibrils can be estimated at 4 (20/4.6) per aggregate for the ancient yarn compared with an average of 6 (30/4.8) for the modern yarn. Considering the hypothesis that the Egyptian flax before ageing had a structure very close to the modern one, the decrease of the number of fibrils for the ancient sample could indicate that some aggregates, especially the larger ones, present in the ancient sample, have been broken off over time. This breakage could result from the degradation of NCPs previously highlighted, particularly galactose, known to be a constituent of RG-I chains playing the role of a gel-matrix in the cellulose microfibrillar ultrastructure and organization (Rihouey et al., 2017): less NCPs including galactose could weaken the ultrastructure and increase the chance of cellulose chains to split off. Those elements are complemented by a schematic representation of the flax cellulose elementary microfibrils structure given in Fig. 5, including calculated parameters from the C4 region deconvolution of ^{13}C CP/MAS spectra from Table 3. Crystalline cellulose (Cr), paracrystalline cellulose (PCr), accessible (AS) and inaccessible (IAS) surfaces were considered.

From those parameters, despite similar crystallinity contents, differences are visible in the amorphous regions: a greater IAS is highlighted for the ancient flax sample (36 vs. 31 %), whereas more AS and PCr are highlighted in modern flax (11 % vs. 7 %, and 37 % vs. 33 % respectively). These results, together with the higher LFAD in modern flax, can illustrate changes in cellulose order level (Villares et al., 2017).

The NMR investigation also involves modelling kinetics of

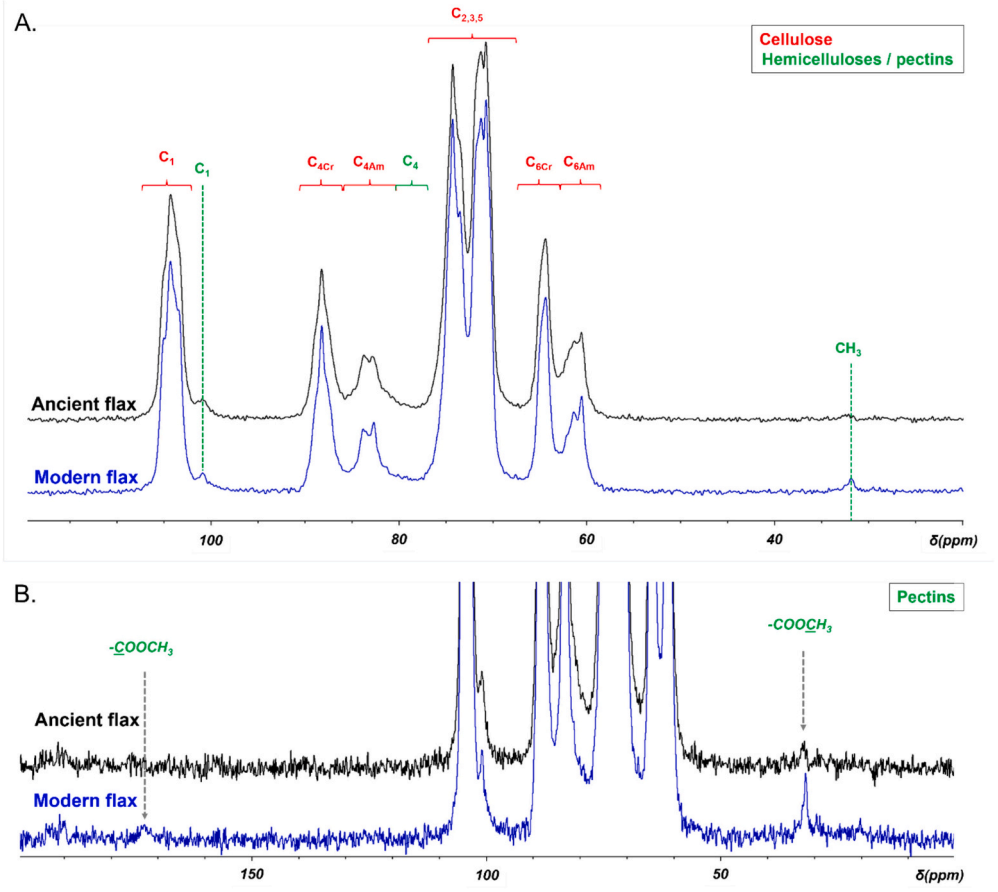

Fig. 4. A. ^{13}C CP/MAS NMR spectra of ancient (in black) and modern (in blue) samples. B. Focus on the lower peaks associated with pectins. The underlined C corresponds to the observed signal.

Table 2
Analysis of cellulose characteristics for ancient and modern samples.

	Cellulose	
	Modern	Ancient
Crystallinity (%)	58	56
Lateral Fibril Dimensions LFD (nm)	4.8	4.6
Lateral Fibril Aggregate Dimensions LFAD (nm)	30	20
Number of fibrils per aggregate	6	4

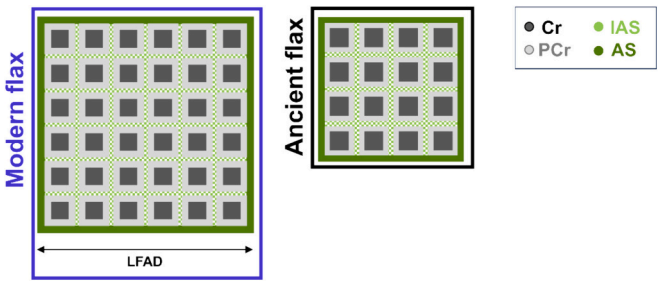

Fig. 5. Schematic representation of an average flax cellulose elementary microfibrils structure from RMN results, for the modern sample and the ancient one. Cr: crystalline cellulose, PCr: paracrystalline cellulose, IAS: inaccessible surface, AS: accessible surface and LFAD: lateral fibril aggregate dimension.

polarization transfer $^{1}H- > {}^{13}C$ using the two-proton reservoir model to analyse the evolution of the crystalline and the amorphous C4 peaks areas as a function of the contact time, for which associated relaxation time values are summarized in Table 4. Based on this table, significantly lower values are obtained in $T_{1\rho}^{H}$ for the ancient yarn, which could be associated with a lower degree of molecular order for this ancient sample (Falourd et al., 2022b). Moreover, the amorphous C4 provides lower values than the crystalline C4. These results indicate that the amorphous components environments are probably more affected by ageing than the crystalline ones. This is consistent with the supposed breakage of large aggregates of cellulose and the increased content of the inaccessible parts in the ancient sample previously mentioned.

Finally, Table 5 provides values obtained using another model proposed by Bardet et al. (Bardet et al., 2012); this model is based on the hypothesis of two domains of molecular organization at the nanoscale. These two domains are associated with a proportion of signals a and b, respectively. If these models have identical $T_{1\rho}^{H}$ values, it indicates homogeneous macromolecular organization at the nanoscale. Here, $T_{1\rho}^{H}$ has two different values only in the modern sample, more particularly in the amorphous region, reflecting probably the existence of two different structural domains at the nanometric scale in modern sample, contrary to the ancient sample, which seems to have a more homogeneous structural organization. This could be linked with the hypothesis that cellulose chains are broken in the ancient sample over time, provoking the local destructuration and homogeneity through disorder. In addition, $T_{1\rho}^{H}$ values for the amorphous region in the modern sample are 56 ms for C4am $T_{\mathbf{a}\rho}^{H}$ and 15 ms for C4am $T_{\mathbf{b}\rho}^{H}$, highlighting a highly structured environment of the amorphous cellulose in zone A. Whereas $T_{1\rho}^{H}$ values are identical and equal to 22 ms for both $T_{\mathbf{a}\rho}^{H}$ and $T_{\mathbf{b}\rho}^{H}$ for the ancient sample showing the loss of global organization for ancient flax (Bourmaud, Siniscalco, et al., 2019). This demonstrates that the amorphous part of the ancient sample is mostly the part of the cellulose which is modified with long-term ageing. Moreover, T_{CH} values are all lower

Table 3
Calculated parameters obtained from the C4 region deconvolution of 13C CP/MAS spectra for ancient and current fibres. δ = chemical shift, FWHH = Full Width at Half Height.

		Cr (Iα)	*Cr (Iα + Iβ)*	*Cr(Iβ)*	*PCr*	*AS*	*IAS*	*AS*
δ (ppm)	***modern***	88.7	88.2	87.5	87.9	83.6	83.1	82.6
	ancient	88.8	88.2	87.6	87.9	83.6	82.9	82.6
FWHH (ppm)	***modern***	0.87	0.45	0.90	2.37	0.90	4.50	0.72
	ancient	0.91	0.47	1.16	2.18	0.87	4.50	0.75
Normalized area (%)	***modern***	7 %	7 %	7 %	37 %	6 %	31 %	5 %
	ancient	9 %	5 %	10 %	33 %	4 %	36 %	3 %

Table 4
Relaxation time values extracted from the two-proton reservoir model for the crystalline and amorphous C4 peaks areas.

	C4am		*C4cr*	
	Modern	Ancient	Modern	Ancient
T_{HH} (μs)	*303*	*280*	*313*	*310*
$T^H_{1\rho}$ (ms)	*32*	*24*	*43*	*34*
T_{CH} (μs)	*14*	*13*	*14*	*14*

Table 5
Parameters extracted from kinetics of polarization transfer for crystalline and amorphous C4 peaks. Standard deviations are given according to literature (Falourd et al., 2022a).

	C4am		*C4cr*	
	Modern	Ancient	Modern	Ancient
a	53 %	50 %	48 %	44 %
$T^H_{a\rho}$ (±2 ms)	*56*	*22*	*35*	*31*
T_{CHa} (±15 μs)	*38*	*32*	*38*	*32*
b	*47 %*	*50 %*	*52 %*	*56 %*
$T^H_{b\rho}$ (±2 ms)	*15*	*22*	*35*	*30*
T_{CHb} (±15 μs)	*499*	*409*	*469*	*396*

for the ancient sample compared to the respective modern ones, in the case of ancient flax. This could be linked with the greater number of kink-bands in the ancient samples (Fig. 1), such defects being known to have cavities and microporosities (Melelli, Durand, et al., 2021) causing moisture ingress and delamination over time. Additionally, cracks, number of kink-bands and local pores observed in Fig. 1. A4-A5 can also be viewed as possible water access to inner cell walls, causing moisture ingress and delamination over time.

Thanks to a multi-scale analysis of biochemical and ultrastructural changes between ancient and modern flax, Fig. 6 synthetizes the main evolutions previously mentioned, i.e. a significant modification of the fibril aggregate dimensions, especially LFAD and aggregate length and, as demonstrated at several scales, a drop in content and structure of pectic components, as well as similarities in terms of hemicellulosic contents.

3.2.2. *Analysis of cell wall indentation modulus through AFM experiments*

Prior to AFM investigations, nanoindentation experiments were conducted. Due to the high penetration depth of the tip in the material and the direct mechanical measurements obtained with this method, nanoindentation helps measure local stiffness, as well as confirm and validate AFM values (Arnould et al., 2017). Indentation modulus and hardness calculated from nanoindentation measurements are in Table 6.

One can notice that similar indentation modulus and hardness are obtained for the two samples; indentation modulus values are fully in line with literature data for modern and ancient flax (Arnould et al., 2017; Melelli, Shah, et al., 2021). For ancient flax, indentation modulus is slightly lower than those obtained for the same textile artefact by Melelli et al. (Melelli, Shah, et al., 2021) but we hypothesize that notable variability exists in the fibre degradation, even in the same yarn; nevertheless, values are in the same range. A more pronounced difference is observed for the hardness with a higher value for the ancient flax; hardness values are generally associated with NCP components and indentation modulus more representative of the behaviour of cellulose (Eder et al., 2013), highlighting here that cellulose could be more preserved than hemicelluloses or pectins, as already discussed after biochemical investigations.

Fig. 7. A. shows the results of AFM investigations with a mapping of the indentation modulus in 2 fibre regions, for the two samples; in

Table 6
Average mechanical properties of ancient and modern fibres obtained by nanoindentation on several fibres.

	Modern	Ancient
Number of values	54	44
Indentation modulus (GPa)	19.0 ± 2.7	18.2 ± 1.3
Hardness (MPa)	400 ± 72	499 ± 25

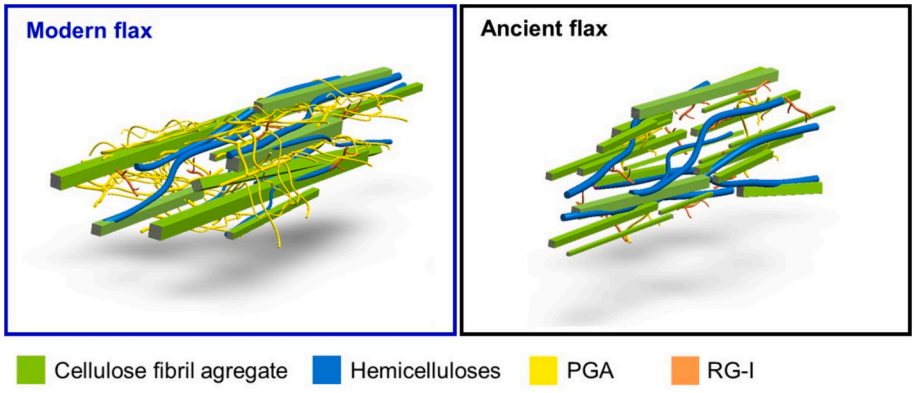

Fig. 6. 3D representation of the flax fibre cell wall structure for modern and ancient samples. A significant decrease in pectin content is evidenced after long-term ageing. In addition, the ultrastructure and size of aggregates of cellulose fibrils is also significantly modified.

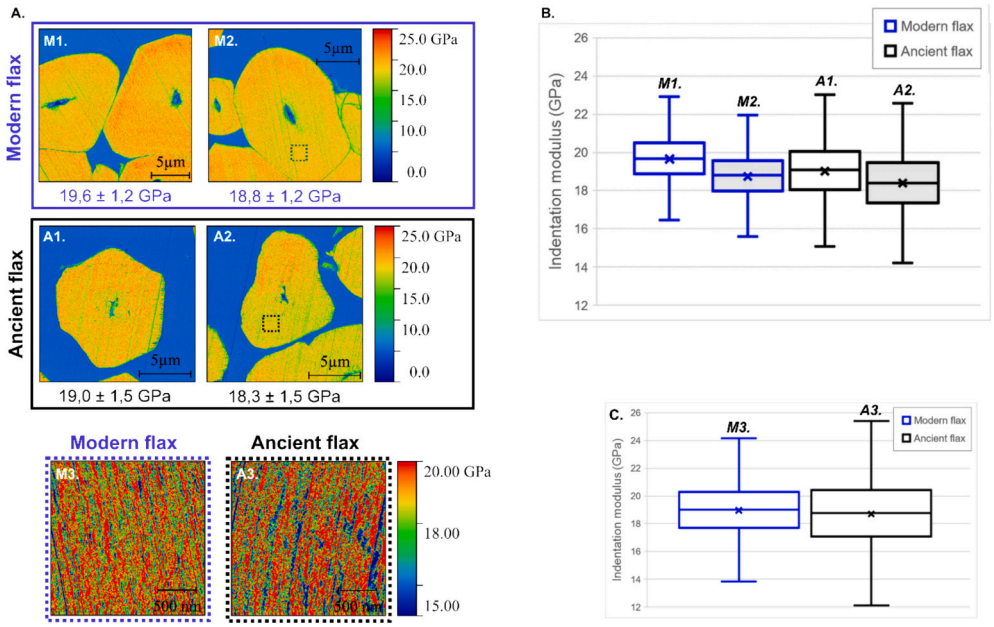

Fig. 7. A. AFM PF-QNM modulus mapping of modern fibres (M1-M2) and ancient ones (A1-A2). Zoom in the G-layer for the modern fibre (M3) and ancient one (A3) (with M3 being the zoom in the zone indicated in M2 and A3 being the zoom in the zone indicated in A2). B. Box-and-whisker boxes showing the data dispersion of the values visible in images M1-M2 and A1-A2. C. Moustache boxes showing the data dispersion of the values visible in images M3 and A3.

addition, a focus in the indicated square zone is provided. These mappings are supplemented by box-and-whisker plots to illustrate the dispersion.

For both modern and ancient samples, AFM indentation moduli are in line with values obtained from nanoindentation investigations. For the 4 mappings carried out at the fibre scale, average values are between 18 and 20 MPa, suggesting that the long-term ageing does not strongly modify the cell wall stiffness. Nevertheless, results appear to be much more heterogenous as evidenced through box-and-whisker plots (Fig. 7. B), suggesting local damages are not clearly visible at this scale. This hypothesis of conservation of stiffness is in good agreement with the previous results and especially the NMR conclusions, indeed, it appears that cellulose crystallinity is not clearly impacted (Table 2) and indentation modulus is considered as an indicator of cellulose behaviour; NMR demonstrates also that the size of fibril aggregates is reduced after ageing, but this is difficult to investigate given the resolution of Fig. 7. A. M1-M2 and A1-A2.

To highlight more details, a zoom is done in two cell wall regions (Fig. 7. M3 and A3) at a reduced scale (2 × 2 µm). A higher heterogeneity in indentation modulus values is evidenced for the ancient flax, reinforced by the box-and-whisker graph (Fig. 7.C). Even, if average values are similar, it appears that ageing influences homogeneity of the sample, suggesting local porosities or components removal. This local degradation corresponds to the low-modulus regions, in blue on Fig. 7. A3. This hypothesis agrees with the findings of the biochemical analyses, which show the loss of several of the main constituents of the walls.

4. Conclusions

This work was dedicated to ultrastructural and mechanical features of flax fibre cell walls after a long-term ageing period. For this, a 4000-year-old sample of Egyptian flax mortuary linen and a modern flax yarn as reference were compared, considering the hypothesis that the Egyptian flax before ageing could be assimilated to the modern one.

In a first step, morphology and state of preservation of fibres were addressed through a detailed SEM analysis; it demonstrated that kink-bands are more intense and numerous on ancient samples and also, that the flax fibres exhibit a more brittle behaviour, with sometimes visible cracks in kink-band regions. The core of the paper is a multi-scale and multi-techniques study with the aim to explore the ultrastructural and chemical changes induced by the ageing, at both the fibre and the cell-wall scale. A significant degradation of elementary components of pectins was highlighted through a detailed sugar analysis, with a drop in galactose and uronic acids content, whereas similarities in the hemicellulose content was confirmed by biochemical analysis and NMR investigations. The ratio between glucose (main component of cellulose) and lignin was quite stable between ancient and modern flax, but synchrotron investigations evidenced by deep-UV spectroscopy that the autofluorescence of lignin is very pronounced in the ancient sample, suggesting a possible quenching of this fluorescence by hemicelluloses for modern samples, this hypothesis being an indirect observation for quantifying NCP degradation. For the ancient flax fibres, a good preservation of cellulose is evidenced, both after crystallinity measurements by NMR and nanomechanical investigations by AFM and nanoindentation, through the remarkable stability of the indentation modulus. Nevertheless, cellulose architecture is modified and especially the dimensions of the fibril aggregates, significantly lower for the ancient flax, suggesting some fragmentation along time.

This piece of work was designed based on a first published work, dedicated to the morphology and structural damages. In forthcoming investigations, it is planned to go further by deeply exploring the damaged region of ancient flax, especially the kink-band regions which are probably the most sensitive areas of the fibres and are preferentially damaged during ageing. For this, specific experimental coupling will be developed, including micro-tomography, tensile testing and also spectroscopic investigations.

CRediT authorship contribution statement

Camille Goudenhooft: Writing – original draft, Methodology, Investigation, Conceptualization. **Alessia Melelli:** Writing – review & editing, Writing – original draft, Methodology, Investigation, Conceptualization. **Sylvie Durand:** Writing – review & editing, Methodology, Investigation. **Xavier Falourd:** Writing – review & editing, Writing – original draft, Methodology, Investigation. **Lucie Le-Bot:** Writing – review & editing, Methodology, Investigation. **Loren Morgillo:** Writing –

review & editing, Methodology, Investigation. **Sanaa Gaballah:** Writing – review & editing, Methodology, Investigation. **Roberta Cortopassi:** Writing – review & editing, Supervision, Resources. **Anita Quiles:** Writing – review & editing, Validation, Supervision, Conceptualization. **Darshil U. Shah:** Writing – review & editing, Validation, Supervision, Conceptualization. **Frédéric Jamme:** Writing – review & editing, Validation, Supervision, Methodology. **Johnny Beaugrand:** Writing – review & editing, Validation, Supervision, Methodology, Conceptualization. **Alain Bourmaud:** Writing – review & editing, Writing – original draft, Validation, Supervision, Methodology, Investigation, Funding acquisition, Conceptualization.

Declaration of competing interest

The authors declare that they have no known competing financial interests or personal relationships that could have appeared to influence the work reported in this paper.

Data availability

Data will be made available on request.

Acknowledgements

The authors gratefully thank the ANR (Agence Nationale de la Recherche) for funding the ANUBIS project (ANR-21-CE43-0010–ANUBIS) and Synchrotron SOLEIL for beamtime on the DISCO beamline (proposal n° 20220511). Méline Calatraba and Anthony Magueresse are also thanked for their experimental contribution.

References

André, J. (1964). Nature du lin et horticulture. In Budé (Ed.), *Pline l'Ancien, Histoire naturelle* (Les Belles).

Arnould, O., Siniscalco, D., Bourmaud, A., Le Duigou, A., & Baley, C. (2017). Better insight into the nano-mechanical properties of flax fibre cell walls. *Industrial Crops and Products, 97*, 224–228. https://doi.org/10.1016/j.indcrop.2016.12.020

Baley, C., Goudenhooft, C., Gibaud, M., & Bourmaud, A. (2018). Flax stems: From a specific architecture to an instructive model for bioinspired composite structures. *Bioinspiration & Biomimetics, 13*(2), Article 026007. https://doi.org/10.1088/1748-3190/aaa6b7

Bardet, M., Gerbaud, G., Doan, C., Giffard, M., Hediger, S., De Paëpe, G., & Trân, Q. K. (2012). Dynamics property recovery of archaeological-wood fibers treated with polyethylene glycol demonstrated by high-resolution solid-state NMR. *Cellulose, 19*(5). https://doi.org/10.1007/s10570-012-9736-y

Basu, S. N., & Ghose, R. (1962). A Microscopical study on the degradation of jute Fiber by Micro-organisms. *Textile Research Journal, 32*(8). https://doi.org/10.1177/004051756203200810

Beaugrand, J., Goudenhooft, C., Alvarado, C., Devaux, M. F., Rivard, C., Durand, S., … Bourmaud, A. (2022). Evolution of the flax cell wall composition during development and after gravitropism by synchrotron fluorescence imaging. *Industrial Crops and Products, 175*. https://doi.org/10.1016/j.indcrop.2021.114256

Blakeney, A. B., Harris, P. J., Henry, R. J., & Stone, B. A. (1983). A simple and rapid preparation of alditol acetates for monosaccharide analysis. *Carbohydrate Research, 113*(2). https://doi.org/10.1016/0008-6215(83)88244-5

Blumenkrantz, N., & Asboe-Hansen, G. (1973). New method for quantitative determination of uronic acids. *Analytical Biochemistry, 54*(2). https://doi.org/10.1016/0003-2697(73)90377-1

Bourmaud, A., Mérotte, J., Siniscalco, D., Le Gall, M., Gager, V., Le Duigou, A., Pierre, F., Behlouli, K., Arnould, O., Beaugrand, J., & Baley, C. (2019). Main criteria of sustainable natural fibre for efficient unidirectional biocomposites. *Composites Part A: Applied Science and Manufacturing, 124*. https://doi.org/10.1016/j.compositesa.2019.105504

Bourmaud, A., Siniscalco, D., Foucat, L., Goudenhooft, C., Falourd, X., Pontoire, B., Arnould, O., Beaugrand, J., & Baley, C. (2019). Evolution of flax cell wall ultrastructure and mechanical properties during the retting step. *Carbohydrate Polymers, 206*, 48–56. https://doi.org/10.1016/j.carbpol.2018.10.065

Bugg, T. D. H., Ahmad, M., Hardiman, E. M., & Rahmanpour, R. (2011). Pathways for degradation of lignin in bacteria and fungi. *Natural Product Reports, 28*(12). https://doi.org/10.1039/c1np00042j

Caneva, G., Nugari, M., & Salvadori, O. (2005). Biodeterioramento e Conservazione. In Nardini (Ed.), *La Biologia vegetale per i beni culturali* (Nardini).

Day, A., Ruel, K., Neutelings, G., Crônier, D., David, H., Hawkins, S., & Chabbert, B. (2005). Lignification in the flax stem: Evidence for an unusual lignin in bast fibers. Planta, 222(2), 234–245. https://doi.org/10.1007/s00425-005-1537-1.

Delafargue, A., & Ulm, F. J. (2004). Explicit approximations of the indentation modulus of elastically orthotropic solids for conical indenters. *International Journal of Solids and Structures, 41*(26), 7351–7360. https://doi.org/10.1016/j.ijsolstr.2004.06.019

Donaldson, L. (2020). Autofluorescence in plants. In *Molecules* (Vol. 25, Issue 10). https://doi.org/10.3390/molecules25102393.

Echard, J. P., Thoury, M., Berrie, B. H., Séverin-Fabiani, T., Vichi, A., Didier, M., … Bertrand, L. (2015). Synchrotron DUV luminescence micro-imaging to identify and map historical organic coatings on wood. *Analyst, 140*(15). https://doi.org/10.1039/c5an00483g

Eder, M., Arnould, O., Dunlop, J. W. C., Hornatowska, J., & Salmén, L. (2013). Experimental micromechanical characterisation of wood cell walls. *Wood Science and Technology, 47*(1). https://doi.org/10.1007/s00226-012-0515-6

Falourd, X., Lahaye, M., & Rondeau-Mouro, C. (2022a). Assessment of cellulose interactions with water by ssNMR: 1H->13C transfer kinetics revisited. *Carbohydrate Polymers, 298*. https://doi.org/10.1016/j.carbpol.2022.120104

Falourd, X., Lahaye, M., & Rondeau-Mouro, C. (2022b). Optimization of acquisition and processing times for the measurement of 1H to 13C polarization transfer kinetics. *MethodsX, 9*. https://doi.org/10.1016/j.mex.2022.101914

Fukushima, R. S., & Hatfield, R. D. (2001). Extraction and isolation of lignin for utilization as a standard to determine lignin concentration using the acetyl bromide spectrophotometric method. *Journal of Agricultural and Food Chemistry, 49*(7). https://doi.org/10.1021/jf010449r

Garat, W., Le Moigne, N., Corn, S., Beaugrand, J., & Bergeret, A. (2020). Swelling of natural fibre bundles under hygro- and hydrothermal conditions: Determination of hydric expansion coefficients by automated laser scanning. *Composites Part A: Applied Science and Manufacturing, 131*. https://doi.org/10.1016/j.compositesa.2020.105803

Garidel, P., Hegyi, M., Bassarab, S., & Weichel, M. (2008). A rapid, sensitive and economical assessment of monoclonal antibody conformational stability by intrinsic tryptophan fluorescence spectroscopy. *Biotechnology Journal, 3*(9–10). https://doi.org/10.1002/biot.200800091

Gassan, J., & Bledzki, A. K. (2001). Thermal degradation of flax and jute fibers. *Journal of Applied Polymer Science, 82*(6). https://doi.org/10.1002/app.1979

Gautreau, M., Durand, S., Paturel, A., Le Gall, S., Foucat, L., Falourd, X., … Beaugrand, J. (2022). Impact of cell wall non-cellulosic and cellulosic polymers on the mechanical properties of flax fibre bundles. *Carbohydrate Polymers, 291*. https://doi.org/10.1016/j.carbpol.2022.119599

Gautreau, M., Kervoelen, A., Barteau, G., Delattre, F., Colinart, T., Pierre, F., Hauguel, M., Le Moigne, N., Guillon, F., Bourmaud, A., & Beaugrand, J. (2021). Fibre individualisation and mechanical properties of a flax-PLA non-woven composite following physical pre-treatments. *Coatings, 11*(7). https://doi.org/10.3390/coatings11070846

Goldberg, R., Morvan, C., Jauneau, A., & Jarvis, M. C. (1996). *Methyl-esterification, de-esterification and gelation of pectins in the primary cell wall* (pp. 151–172). https://doi.org/10.1016/S0921-0423(96)80253-X.

Gorshkova, T., & Morvan, C. (2006). Secondary cell-wall assembly in flax phloem fibres: Role of galactans. *Planta, 223*(2), 149–158. https://doi.org/10.1007/s00425-005-0118-7

Gorshkova, T. A., Gurjanov, O. P., Mikshina, P. V., Ibragimova, N. N., Mokshina, N. E., Salnikov, V. V., … Chemikosova, S. B. (2010). Specific type of secondary cell wall formed by plant fibers [journal article]. *Russian Journal of Plant Physiology, 57*(3), 328–341. https://doi.org/10.1134/S1021443710030040

Goudenhooft, C., Bourmaud, A., & Baley, C. (2019). Flax (Linum usitatissimum L.) fibers for composite reinforcement: Exploring the link between plant growth, cell walls development, and fiber properties. *Frontiers. Plant Science, 10*(April), 1–23. https://doi.org/10.3389/fpls.2019.00411

Goudenhooft, C., Siniscalco, D., Arnould, O., Bourmaud, A., Sire, O., Gorshkova, T., & Baley, C. (2018). Investigation of the mechanical properties of flax cell walls during plant development: The relation between performance and cell wall structure. *Fibers, 6*(1), 6. https://doi.org/10.3390/fib6010006

Guillou, E., Dumazert, L., Caër, C., Beigbeder, A., Ouagne, P., Le Saout, G., Beaugrand, J., Bourmaud, A., & Le Moigne, N. (2023). In-situ monitoring of changes in ultrastructure and mechanical properties of flax cell walls during controlled heat treatment. *Carbohydrate Polymers, 321*, Article 121253. https://doi.org/10.1016/j.carbpol.2023.121253

Hafrén, J. (2007). Excitation wavelength-specific changes in lignocellulosic autofluorescence. *Journal of Wood Science, 53*(4). https://doi.org/10.1007/s10086-006-0862-8

Hammer, Ø., Harper, D. A. T., & Ryan, P. D. (2001). Past: Paleontological statistics software package for education and data analysis. *Palaeontologia Electronica, 4*(1).

Hatfield, R., & Fukushima, R. S. (2005). Can lignin be accurately measured? *Crop Science, 45*(3). https://doi.org/10.2135/cropsci2004.0238

Heer, O. (1873). Prehistoric culture of flax. *Nature, 453*. https://doi.org/10.1038/007453a0

Iiyama, K., & Wallis, A. F. A. (1990). Determination of lignin in herbaceous plants by an improved acetyl bromide procedure. *Journal of the Science of Food and Agriculture, 51*(2). https://doi.org/10.1002/jsfa.2740510202

Jäger, A., Bader, T., Hofstetter, K., & Eberhardsteiner, J. (2011). The relation between indentation modulus, microfibril angle, and elastic properties of wood cell walls. *Composites Part A: Applied Science and Manufacturing, 42*(6), 677–685. https://doi.org/10.1016/j.compositesa.2011.02.007

Jamme, F., Kascakova, S., Villette, S., Allouche, F., Pallu, S., Rouam, V., & Réfrégiers, M. (2013). Deep UV autofluorescence microscopy for cell biology and tissue histology. *Biology of the Cell, 105*(7), 277–288. https://doi.org/10.1111/boc.201200075

Jamme, F., Villette, S., Giuliani, A., Rouam, V., Wien, F., Lagarde, B., & Réfrégiers, M. (2010). Synchrotron UV fluorescence microscopy uncovers new probes in cells and

tissues. *Microscopy and Microanalysis, 16*(5). https://doi.org/10.1017/S1431927610093852
Lahaye, M., Thoulouze, L., Calatraba, M., Gauclain, T., Falourd, X., Le-Quere, J. M., … Bauduin, R. (2023). A multimodal and multiscale investigation of factors affecting the juice yield of cider apples. *Food Chemistry, 420*. https://doi.org/10.1016/j.foodchem.2023.135649
Lakowicz, J. R. (2006). Principles of fluorescence spectroscopy. *In Principles of Fluorescence Spectroscopy.*. https://doi.org/10.1007/978-0-387-46312-4
Larsson, P. T., Wickholm, K., & Iversen, T. (1997). A CP/MAS 13C NMR investigation of molecular ordering in celluloses. *Carbohydrate Research, 302*(1–2). https://doi.org/10.1016/S0008-6215(97)00130-4
Lashermes, G., Bleuze, L., Recous, S., Voinot, R., Lafolie, F., & Chabbert, B. (2020). Multiscale modeling of microbial degradation of outer tissues of fiber-crop stems during the dew retting process. *Bioresource Technology, 311*. https://doi.org/10.1016/j.biortech.2020.123558
Le Duigou, A., & Castro, M. (2016). Evaluation of force generation mechanisms in natural, passive hydraulic actuators. *Scientific Reports, Accepted(JANUARY)*, 1–9. https://doi.org/10.1038/srep18105
Melelli, A., Arnould, O., Beaugrand, J., & Bourmaud, A. (2020). The middle lamella of plant fibers used as composite reinforcement: Investigation by atomic force microscopy. *Molecules, 25*(3). https://doi.org/10.3390/molecules25030632
Melelli, A., Durand, S., Alvarado, C., Kervoëlen, A., Foucat, L., Grégoire, M., Arnould, O., Falourd, X., Callebert, F., Ouagne, P., Geairon, A., Daniel, S., Jamme, F., Mauve, C., Gakière, B., Bourmaud, A., & Beaugrand, J. (2022). Anticipating global warming effects: A comprehensive study of drought impact of both flax plants and fibres. *Industrial Crops and Products, 184*, Article 115011. https://doi.org/10.1016/j.indcrop.2022.115011
Melelli, A., Durand, S., Arnould, O., Richely, E., Guessasma, S., Jamme, F., Beaugrand, J., & Bourmaud, A. (2021). Extensive investigation of the ultrastructure of kink-bands in flax fibres. *Industrial Crops and Products, 164*. https://doi.org/10.1016/j.indcrop.2021.113368
Melelli, A., Jamme, F., Legland, D., Beaugrand, J., & Bourmaud, A. (2020). Microfibril angle of elementary flax fibres investigated with polarised second harmonic generation microscopy. *Industrial Crops and Products, 156*. https://doi.org/10.1016/j.indcrop.2020.112847
Melelli, A., Pantaloni, D., Balnois, E., Arnould, O., Jamme, F., Baley, C., … Bourmaud, A. (2021). Investigations by AFM of ageing mechanisms in PLA-flax fibre composites during garden composting. *Polymers, 13*(14). https://doi.org/10.3390/polym13142225
Melelli, A., Roselli, G., Proietti, N., Bourmaud, A., Arnould, O., Jamme, F., … Santulli, C. (2021). Chemical, morphological and mechanical study of the ageing of textile flax fibers from 17th/18th-century paintings on canvas. *Journal of Cultural Heritage, 52*, 202–214. https://doi.org/10.1016/j.culher.2021.10.003
Melelli, A., Shah, D. U., Hapsari, G., Cortopassi, R., Durand, S., Arnould, O., … Bourmaud, A. (2021). Lessons on textile history and fibre durability from a 4,000-year-old Egyptian flax yarn. *Nature Plants, 7*(9), 1200–1206. https://doi.org/10.1038/s41477-021-00998-8
Morvan, C., Andème-Onzighi, C., Girault, R., Himmelsbach, D. S., Driouich, A., & Akin, D. E. (2003). Building flax fibres: More than one brick in the walls. *Plant Physiology and Biochemistry, 41*(11−12), 935–944. https://doi.org/10.1016/j.plaphy.2003.07.001
Newman, R. H. (1999). Estimation of the lateral dimensions of cellulose crystallites using 13C NMR signal strengths. *Solid State Nuclear Magnetic Resonance, 15*(1). https://doi.org/10.1016/S0926-2040(99)00043-0
Newman, R. H., Battley, M. A., Carpenter, J. E. P., & Le Guen, M. J. (2012). Energy loss in a unidirectional flax-polyester composite subjected to multiple tensile load-unload cycles. *Journal of Materials Science, 47*(3). https://doi.org/10.1007/s10853-011-5713-3
Newman, R. H., & Redgwell, R. J. (2002). Cell wall changes in ripening kiwifruit: 13C solid state NMR characterisation of relatively rigid cell wall polymers. *Carbohydrate Polymers, 49*(2). https://doi.org/10.1016/S0144-8617(01)00323-X
Nuez, L., Durand, S., Melelli, A., Berrin, J.-G., Haon, M., Drula, E., … Baley, C. (2022). Exploring the impact of Verticillium wilt disease on the mechanical properties of elementary flax (Linum usitatissimum L.) fibres. *Industrial Crops and Products, 182*, Article 114900. https://doi.org/10.1016/j.indcrop.2022.114900
Oliver, W. C., & Pharr, G. M. (1992). An improved technique for determining hardness and elastic modulus using load and displacement sensing indentation experiments. *Journal of Materials Research, 7*(6). https://doi.org/10.1557/jmr.1992.1564
Peacock, E. E. (1983). Deacidification of degraded linen. *Studies in Conservation, 28*(1). https://doi.org/10.1179/sic.1983.28.1.8
Poulon, F., Jamme, F., Ibrahim, A., Métais, C., Varlet, P., Juchaux, M., Devaux, B., Refregiers, M., & Haidar, D. A. (2017). Endogenous fluorescence analysis under deep UV excitation to discriminate human brain tumor tissue: Difference between glioblastoma and healthy control tissue. *PHOTOPTICS 2017 - proceedings of the 5th international conference on photonics, optics and laser technology*, *2017-January*. https://doi.org/10.5220/0006103601520157.
Rihouey, C., Paynel, F., Gorshkova, T., & Morvan, C. (2017). Flax fibers: Assessing the non-cellulosic polysaccharides and an approach to supramolecular design of the cell wall. *Cellulose, 24*(5), 1985–2001. https://doi.org/10.1007/s10570-017-1246-5
Salvant, J., Barthel, E., & Menu, M. (2011). Nanoindentation and the micromechanics of van Gogh oil paints. *Applied Physics A: Materials Science and Processing, 104*(2). https://doi.org/10.1007/s00339-011-6486-x
Siniscalco, D., Arnould, O., Bourmaud, A., Le Duigou, A., & Baley, C. (2018). Monitoring temperature effects on flax cell-wall mechanical properties within a composite material using AFM. *Polymer Testing, 69*, 91–99. https://doi.org/10.1016/j.polymertesting.2018.05.009
Tiennot, M., Paardekam, E., Iannuzzi, D., & Hermens, E. (2020). Mapping the mechanical properties of paintings via nanoindentation: A new approach for cultural heritage studies. *Scientific Reports, 10*(1). https://doi.org/10.1038/s41598-020-64892-7
Toplak, M., Birarda, G., Read, S., Sandt, C., Rosendahl, S. M., Vaccari, L., … Borondics, F. (2017). Infrared Orange: Connecting hyperspectral data with machine learning. *Synchrotron Radiation News, 30*(4). https://doi.org/10.1080/08940886.2017.1338424
Toplak, M., Read, S. T., Sandt, C., & Borondics, F. (2021). Quasar: Easy machine learning for biospectroscopy. *Cells, 10*(9). https://doi.org/10.3390/cells10092300
Vidot, K., Devaux, M. F., Alvarado, C., Guyot, S., Jamme, F., Gaillard, C., … Lahaye, M. (2019). Phenolic distribution in apple epidermal and outer cortex tissue by multispectral deep-UV autofluorescence cryo-imaging. *Plant Science, 283*. https://doi.org/10.1016/j.plantsci.2019.02.003
Villares, A., Moreau, C., Bennati-Granier, C., Garajova, S., Foucat, L., Falourd, X., … Cathala, B. (2017). Lytic polysaccharide monooxygenases disrupt the cellulose fibers structure. *Scientific Reports, 7*. https://doi.org/10.1038/srep40262
Vogelsang-Eastwood, G. (2000). Textiles. In P. T. Nicholson, & I. Shaw (Eds.), *Ancient Egyptian materials and technology*. Cambridge University Press Cambridge. doi:LK https://worldcat.org/title/38542531.
van Zeist, W., & Bakker-Heeres, J. A. H. (1975). Evidence for linseed cultivation before 6000 bc. *Journal of Archaeological Science, 2*(3). https://doi.org/10.1016/0305-4403(75)90059-X
Zuckerstätter, G., Schild, G., Wollboldt, P., Röder, T., Weber, H. K., & Sixta, H. (2009). The elucidation of cellulose supramolecular structure by 13C CP-MAS NMR. *Lenzinger Berichte, 87*(January), 38–46.